BRAIN
ORIGINAL ARTICLE

The biomechanical signature of loss of consciousness: computational modelling of elite athlete head injuries

Karl. A. Zimmerman,[1,2,3] Janie Cournoyer,[4] Helen Lai,[1,2] Samuel B. Snider,[5] David Fischer,[6] Simon Kemp,[7,8] Clara Karton,[4] Thomas B. Hoshizaki,[4] Mazdak Ghajari[3] and David J. Sharp[1,2,9]

Sports related head injuries can cause transient neurological events including loss of consciousness and dystonic posturing. However, it is unknown why head impacts that appear similar produce distinct neurological effects. The biomechanical effect of impacts can be estimated using computational models of strain within the brain.

Here, we investigate the strain and strain rates produced by professional American football impacts that led to loss of consciousness, posturing or no neurological signs. We reviewed 1280 National Football League American football games and selected cases where the team's medical personnel made a diagnosis of concussion. Videos were then analysed for signs of neurological events. We identified 20 head impacts that showed clear video signs of loss of consciousness and 21 showing clear abnormal posturing. Forty-one control impacts were selected where there was no observable evidence of neurological signs, resulting in 82 videos of impacts for analysis. Video analysis was used to guide physical reconstructions of these impacts, allowing us to estimate the impact kinematics. These were then used as input to a detailed 3D high-fidelity finite element model of brain injury biomechanics to estimate strain and strain rate within the brain.

We tested the hypotheses that impacts producing loss of consciousness would be associated with the highest biomechanical forces, that loss of consciousness would be associated with high forces in brainstem nuclei involved in arousal and that dystonic posturing would be associated with high forces in motor regions.

Impacts leading to loss of consciousness compared to controls produced higher head acceleration (linear acceleration; $81.5\,g \pm 39.8$ versus 47.9 ± 21.4; $P = 0.004$, rotational acceleration; $5.9\,krad/s^2 \pm 2.4$ versus 3.5 ± 1.6; $P < 0.001$) and in voxel-wise analysis produced larger brain deformation in many brain regions, including parts of the brainstem and cerebellum. Dystonic posturing was also associated with higher deformation compared to controls, with brain deformation observed in cortical regions that included the motor cortex. Loss of consciousness was specifically associated with higher strain rates in brainstem regions implicated in maintenance of consciousness, including following correction for the overall severity of impact. These included brainstem nuclei including the locus coeruleus, dorsal raphé and parabrachial complex.

The results show that in head impacts producing loss of consciousness, brain deformation is disproportionately seen in brainstem regions containing nuclei involved in arousal, suggesting that head impacts produce loss of consciousness through a biomechanical effect on key brainstem nuclei involved in the maintenance of consciousness.

1 UK Dementia Research Institute, Care Research & Technology Centre, Imperial College London, London, UK
2 Department of Brain Sciences, Hammersmith Hospital, Imperial College London, London, UK
3 HEAD Lab, Dyson School of Design Engineering, Imperial College London, London, UK
4 Neurotrauma Impact Science Laboratory, University of Ottawa, Ottawa, ON, Canada

Received June 17, 2022. Revised November 17, 2022. Accepted December 02, 2022. Advance access publication December 22, 2022

5 Division of Neurocritical care, Department of Neurology, Brigham and Women's Hospital and Harvard Medical School, Boston, MA, USA
6 Division of Neurocritical Care, Department of Neurology, University of Pennsylvania, Philadelphia, PA, USA
7 Rugby Football Union, Twickenham, UK
8 London School of Hygiene and Tropical Medicine, London, UK
9 The Royal British Legion Centre for Blast Injury Studies and the Department of Bioengineering, Imperial College London, London, UK

Correspondence to: David Sharp
UKDRI Care Research and Technology Centre
Sir Michael Uren Hub, Imperial College London
86 Wood Lane, London W12 0BZ, UK
E-mail: david.sharp@imperial.ac.uk

Correspondence may also be addressed to: Mazdak Ghajari
Dyson School of Design Engineering, Imperial College London
South Kensington, London SW7 2AZ, UK
E-mail: m.ghajari@imperial.ac.uk

Keywords: TBI; biomechanics; loss of consciousness; sports tbi; concussion

Introduction

There are 45 to 54 million mild traumatic brain injuries (mTBI) a year globally.[1] These can be associated with loss of consciousness (LOC) and other focal neurological signs, including abnormal motor posturing. These effects are apparent in professional sports, where they are used to identify suspected concussion and trigger removal from play decisions.[2,3] However, it is unclear why impacts that can appear superficially similar produce very different immediate neurological outcomes. Distinct neurological signs are likely to reflect transient dysfunction in specific brain regions produced by the biomechanical effects of the head impacts. Hence, understanding the biomechanical effects of head impacts within the brain is likely to be informative and provides a way to quantify TBI severity.[4-6] The magnitude and distribution of these biomechanical forces in the brain are known to contribute to the severity of the injury,[7] and initial results suggest LOC involves a greater degree of tissue deformation in the brain[8,9] It is unknown how the spatial patterns of deformation relate to specific neurological signs that are produced.

Loss of consciousness is characterized by complete loss of motor tone and can be reliably identified with video review or via pitchside surveillance. Similarly, abnormal posturing can also be identified, as abnormal motor activity produces a 'fencing' response seen either unilaterally or bi-laterally. Medical staff and dedicated 'concussion-spotters' are increasingly used to identify these features in sports including American football or rugby.[10] Reported rates of LOC in mTBIs from professional sports range from 6.4 to 8.8%.[11,12] The frequency of posturing that is reported is more variable, with a rate of 7.1% in rugby[13] and 35.2% in a select review of professional American football concussions from 2013–15.[14] It is not clear if neurological events at the time of injury are indicative of poorer long term outcomes. Posturing is generally thought to be relatively benign, with an absence of related long-term imaging or cognitive impairments.[15-17] Evidence for LOC is mixed, as some studies also report that LOC is not associated with poorer outcomes or cognitive impairment,[18-20] although others show worse cognitive performance and an increased probability of radiological abnormalities post-LOC.[21,22]

Head impacts can produce biomechanical effects within the brain stem that may be particularly relevant to understanding LOC. Experimental injuries in cats show damage to the reticular formation within the brainstem produces coma.[23,24] More recent human work has shown that lesions in the brainstem tegmentum are highly predictive of prolonged LOC.[25,26] The brainstem tegmentum contain neuromodulatory nuclei, including cholinergic, dopaminergic and noradrenergic neurons involved in arousal and alertness.[27,28] Damage to the dorsal raphé or locus coeruleus is prominent after severe TBI and can be associated with impaired arousal.[29] Loss of consciousness from a head impact may therefore be a result of biomechanical effects within these specific brainstem nuclei or their cortical projections which are particularly vulnerable to mechanical loading, including the shear, tensile and compressive forces that are generated as a result of mTBIs.[30-32]

Dystonic posturing may result from transient dysfunction with the motor system. This can occur with or without LOC, probably because the biomechanical effects of an impact differentially affect the motor and arousal systems.[16,33] Dystonic posturing is not thought to be epileptic in origin, but rather due to a transient physiological change, perhaps produced by a reduction in cortical inhibition.[34] Hence, impacts leading to LOC and posturing may result from distinct biomechanical effects on the motor and arousal systems.

Finite element modelling can be used to investigate the pattern of biomechanical forces in the brain produced by head impacts.[6,8,9,35-42] These models incorporate mechanical tissue properties[43] and have been validated using cadaver and animal models of TBI.[6,44] We have developed a high-fidelity finite element model that has been used to predict patterns of strain and strain rate produced by a range of head impacts with high spatial resolution.[6,37,38] Controlled cortical impact modelling in the rat has been used to validate this approach. This work shows that estimates of strain and strain rates produced by the impact correlated with histopathological and MRI markers of axonal, glial injury and blood–brain barrier damage.[6,36] In humans, the model has been used to investigate sporting impacts, falls and road

traffic accidents, showing high strain and strain rates in the depths of sulci at points of anatomical gyral inflection where tau pathology is observed in cases of chronic traumatic encephalopathy.[37,38] A version of this model that contains a definition of the anatomy of the venous system has also been developed[36] and has been used to predict the location of microbleeds after head impact in sports.[35]

Here, we performed detailed investigation of 82 head impacts from professional adult male American football players and investigated differences in the magnitude and distribution of brain deformation from impacts that led to LOC, posturing or produced no observable immediate neurological signs. Previous work has shown that impacts leading to neurological signs (LOC and posturing) are associated with a general increase in brain deformation,[9] with the highest deformation reported to be in the cerebral white matter for LOC impacts.[39] However, computational models used previously have lacked the anatomical features and resolution to investigate the spatial distribution of brain deformation in detail. In addition, we have been able to apply advanced statistical techniques derived from neuroimaging to investigate the biomechanical correlates of clinical features of mTBI using a highly anatomically detailed 3D model of TBI biomechanics. This allows a detailed evaluation of strain and strain rate magnitude and distribution differences between groups. Here we specifically test the hypotheses that: (i) impacts leading to LOC will be associated with higher strains and strain rates across the brain; (ii) these forces will be particularly high within the brainstem in impacts leading to LOC; and (iii) impacts leading to posturing will be associated with high strain in the motor cortex and/or corticospinal tracts.

Materials and methods

Case selection

The method for case selection of impacts has been described previously.[9] A total of 1280 elite American football games over a 5-year period were reviewed for concussive head injuries, defined based on the diagnosis of a 'concussion' by the team's medical personnel and communication through associated press releases. Videos of impacts leading to the injury were then analysed for observable signs of neurological events (Fig. 1A). Loss of consciousness was defined as impacts leading to a player displaying a complete loss of motor tone or a failure to protect themselves during the ensuing fall within the first 2 s after impact. Posturing was defined as impacts leading to flexion or extension in the upper or lower extremities in any combination, and did not fit the criteria for LOC. In cases where the neurological events could not be confirmed, cases were excluded from the study. We also defined specific control impacts that were event matched (e.g. a fall, or shoulder/helmet to helmet collision) to impacts in the LOC and posturing group. These impacts were concussive head injury events, as defined earlier, that did not produce any visible signs on video, i.e. posturing or LOC. All concussive impacts preceded players being removed from play. This allowed for the identification of the injurious impact in the control group. Control impacts were selected using a random number generator to select control cases from a range of impacts that matched the collision characteristics of the LOC and posturing group cases, i.e. if a shoulder-to-helmet impact produced LOC, then a similar type of impact was selected at random from all the examples of shoulder-to-helmet impacts in the control dataset. In total, 20 LOC cases, 21 posturing cases and 41 impacts leading to no visible signs (control cases) were included in this study. Return to play duration was defined as the time after which players returned to a game or were allowed full contact as stated in a press release. For subgroup analysis, players were grouped into either fewer than 14 days required for return to play, or 14 days or more for subgroup analysis, consistent with definitions for persistent post-traumatic symptoms in adults.[45]

Video screening and laboratory reconstructions

The methodologies involved in video analysis and laboratory reconstructions of head impacts have been described previously in detail.[39,46] In brief, videos were first screened for suitability of physical reconstruction. Videos required a clear view of the impact and distinguishable pitch markings to allow for calibration of distances on video to known pitch dimensions. Kinovea (version 0.8.20) was used to calculate impact velocity by determining the distance between the injured players head and impacting surface 0.04–0.2 s prior to impact (Fig. 1B). This method yields measurement errors of less than 10% in ice hockey[47] and is likely to be similar or smaller in American football due to the increased number of markings on the field to establish a more accurate calibration. Furthermore, videos of professional American football include a larger number of cameras, with angles typically perpendicular to the field, increasing the field of view and accuracy of the measurement. Head location/orientation and event type was also recorded from video footage.

These parameters were used to guide physical reconstructions of the head impact events at the University of Ottawa using a Hybrid III 50th-percentile adult male headform and neutral unbiased neckform, which performs similarly to a Hybrid III neck without a directional bias (Fig. 1C).[48] Mounted accelerometers were used to capture linear and rotational acceleration of the head during an impact. The headform was equipped with an American football helmet with matching liners based on helmets worn at the time of impact. Helmet-to-helmet collisions were simulated using a 15.9 kg impacting arm wearing an American football helmet. In cases of shoulder-to-helmet impacts, a 13 kg impact arm with an American football shoulder pad was used.

Finite element brain modelling

The Imperial College London 3D finite element model of the human head (IC 1.0) was used to calculate brain deformations from each head impact. The model was developed using high-resolution MRI of a healthy 34-year-old male subject and consists of nearly one million hexahedral elements and a quarter of a million quadrilateral elements. Briefly, we used an image-based mesh generation approach to develop the head FE mesh, similar to previous work.[41,49] We segmented the T_1-weighted image of the subject into skin, skull, CSF, grey matter, white matter, ventricles and brainstem using Freesurfer and FSL.[50,51] Each voxel of the image was replaced with a hexahedral element (1.5 mm edge length) using an in-house code. The falx and tentorium were added between the hemispheres and cerebrum/cerebellum, respectively, using shell elements. A layer of shell elements was added on the grey matter to represent the pia matter. The mesh at the interface between CSF/skull and grey matter/CSF was smoothed, but we did not smooth the mesh at the interface between grey matter and white matter, because they had the same material properties. The final model had an average element size of 1.5 mm, with 0.1 mm for the smallest element, representing 11 tissues, including the scalp, skull, brain, meninges, subarachnoid space and ventricles, as well as anatomical features

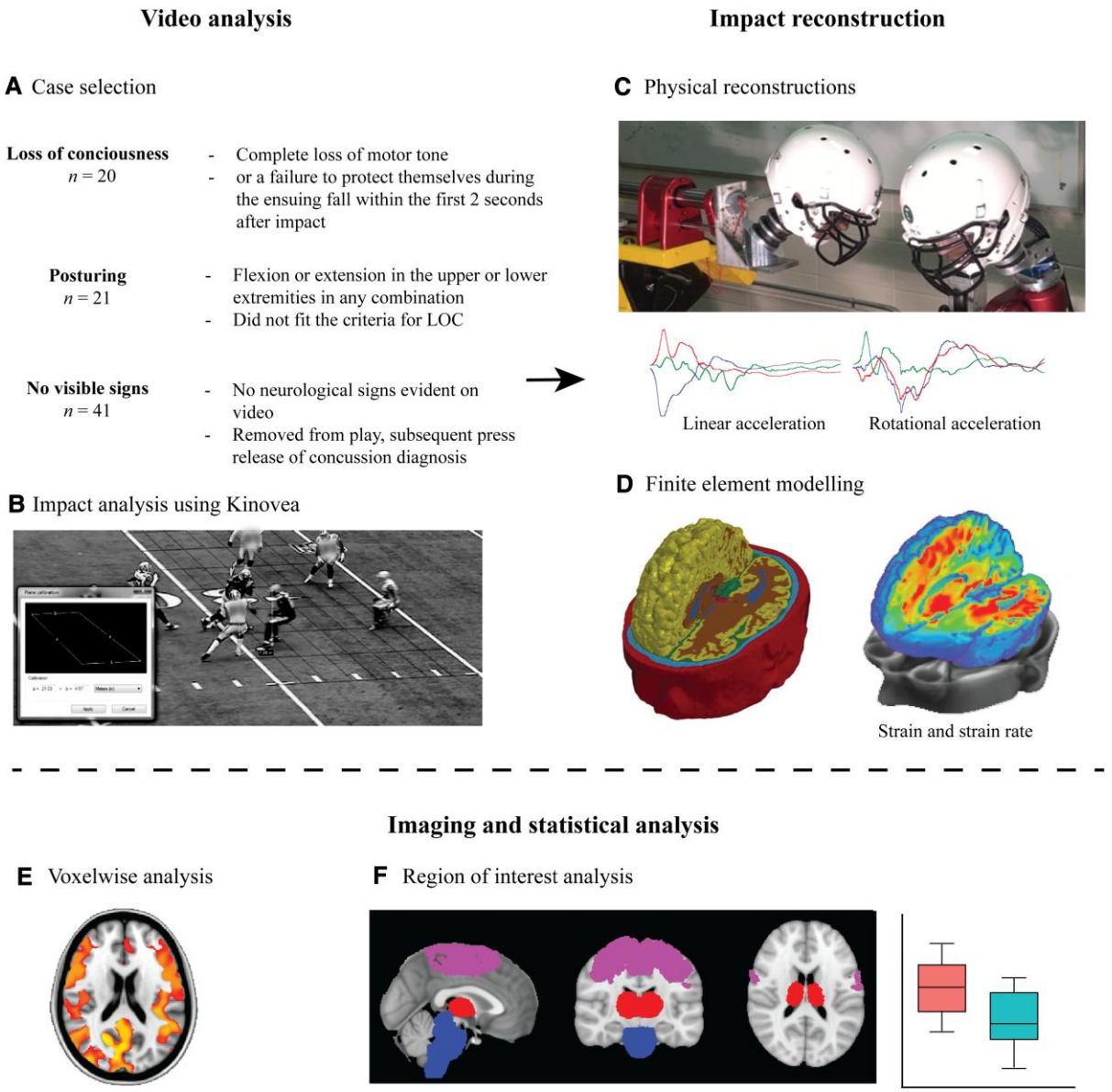

Figure 1 Methods and workflow. Videos of professional American football games were analysed to select cases of (**A**) players who lost consciousness, experienced dystonic posturing or did not show any visible signs of injury but were later diagnosed with a concussion by a team's medical professional. (**B**) Impacts were analysed using Kinovea and (**C**) were physically reconstructed in a lab to estimate the accelerations of the head during the impact. (**D**) Information on head acceleration was then used as input for finite element modelling of the biomechanics of the injury, producing metrics such as strain and strain rate. (**E**) Biomechanical metrics were then analysed using neuroimaging techniques such as voxel-wise analyses, and (**F**) region of interest analysis was performed to test specific hypotheses.

such as sulci. The model predictions of brain displacement were validated against recently published experimental data from well-documented and open-access post-mortem human subject (PMHS) experiments.[44,52] In short, controlled rotational motion was applied to a PMHS head, with crystals inserted to allow for measuring displacement time histories. These were compared to model predictions using the LS-DYNA CORA (CORrelation and Analysis) to assess prediction fidelity (with acceptable threshold defined as CORA > 0.44). The mean CORA for all tests and axes range from 0.50 to 0.65, which indicates an overall fair fidelity of the predictions. Further detail on the model material characteristics, development details and validation are described in previous work[37,38] and in Supplementary Figs 1–5 and Supplementary Tables 1–2.

The finite element head model was loaded by linear and rotational accelerations obtained from the physical reconstructions of the impacts (Fig. 1D). For each element of the model, we determined the maximum principal value of the Green–Lagrange strain tensor (E), a measure of how much the element has been stretched with respect to its original shape (hereafter labelled as strain). We also calculate the maximum principal value of the total time derivative of the Green–Lagrange strain tensor that the element experienced during the simulation, which is a measure of the maximum time rate of stretch within each element (hereafter labelled as the strain rate).[53] Values for strain and strain rate were encoded in a voxel-wise basis and saved as a NIFTI (Neuroimaging Informatics Technology Initiative) file for neuroimaging analysis.

Modelling predictions—neuroimaging analysis

Strain and strain rate data for each impact were analysed using fMRIB Software Library (FSL) v6.0.2. Whole brain measures of strain and strain rates were defined as the 90th percentile value of strain and strain rate sampled from voxels across the whole brain. This was done to account for possible abnormally large strains in poorly defined elements and represents the peak strain and strain-rate values reached across the whole brain during an impact. Strain and strain rate images were merged and means calculated at each voxel across all impacts per neurological event type. Voxel-wise analysis was conducted using the general linear model with non-parametric permutation testing (10 000) in FSL Randomise,[54] and results reported are threshold-free cluster enhancement (TFCE)-corrected for multiple comparisons at a threshold of $P < 0.05$ (Fig. 1E). A secondary voxel-wise analysis was repeated but with 90th percentile strain and strain rates used as covariates to investigate proportional spatial differences. Region of interest analysis was conducted after registering strain and strain rate images to MNI152 space, and sampling from within masks of the thalamus, brainstem and motor cortex. Thalamus, brainstem and supplementary motor area masks were derived from the Harvard–Oxford brain atlas,[55] while the motor cortex atlas was derived from the primary and pre-motor masks from the Jülich histological atlas.[56] Corpus callosum and corticospinal tract regions of interest were derived from the ICBM-81-DTI white matter atlas.[57] Left and right anterior thalamic radiation regions were derived from the JHU white-matter tractography atlas[58] and motor areas determined to be associated with upper limb function from the brainnetome atlas.[59] The Harvard AAN atlas was used to identify brainstem nuclei in Montreal Neurological Institute (MNI) space.[60]

Comparison with brainstem lesions causing loss of consciousness

We compared areas of significant brainstem deformation from voxel-wise analyses with regions of interest identified from previous studies of lesions leading to LOC. A comparison was made with a coma-specific brainstem region, identified from an analysis of brainstem lesions that either did or did not cause coma.[26] A second comparison was made with a brainstem region identified based on preferential functional connectivity to penetrating traumatic cortical lesions in patients that did or did not have LOC.[25] Relevant methods for lesion analyses can found in their respective publications.

Statistical analysis

Statistical tests were completed in the open-source software package R. The comparison of proportion of lateralized impacts, impact location and return to play classification between groups was completed using a Pearson's χ^2 test. Peak resultant linear and rotational acceleration and velocities were calculated from accelerations and velocities in the x, y and z plane. Head kinematics including linear and rotational velocity and acceleration, whole brain deformation measures including 90th percentile strain and strain rate and region of interest analysis of mean strain and strain rates were tested for normality using the Shapiro–Wilk test for normality and Levene's tests was used to assess homogeneity of variances across groups. Due to the tests violating the normality assumption, comparisons of all head kinematic data and whole brain deformations were done using the non-parametric Kruskal–Wallis H tests, which can accommodate both parametric and non-parametric data, with pairwise Wilcoxon rank sum tests and false discovery rate (FDR) correction for *post hoc* analysis. A Pearson's correlation was used to test the correlation between 90th percentile strain and strain rate. Voxel-wise imaging statistical analysis to test whether there were differences between impacts leading to different neurological events was used as described above. Group differences in impact kinematics and brain deformation between players with return to play durations greater or less than 14 days long were investigated using two-sided Student's *t*-tests. A *P*-value threshold for reporting of <0.05 was used.

Data availability

The processed kinematics, simulation and clinical data that support the findings of this study are available from the corresponding author upon request.

Results

Eighty-two head impacts were investigated: 20 produced LOC, 21 dystonic posturing and 41 control impacts had no visible neurological signs (Supplementary Table 3). Impacts occurred to both the left side of the head ($n = 40$) and right ($n = 29$), and more were lateralized (left or right, $n = 70$) compared to direct (front or back, $n = 12$). Posturing was seen in both limbs bilaterally in 15 cases, with a higher number of impacts to the left ($n = 12$) than right ($n = 6$) side of the head. A comparison of the groups showed no differences in impact location ($P = 0.82$) or proportion of impacts that were direct compared to lateralized ($P = 0.76$). Voxel-wise analysis showed no differences in strain between impact location groups. There was no relationship between the side of the head impacted and lateralization of dystonic posturing. There was also no difference in the proportion of individuals who had a return to play within, or longer than 2 weeks between the groups ($P = 0.63$).

Case studies

Physical reconstructions of the impacts produced kinematic measures of peak linear and rotational accelerations. Illustrative cases are shown in Fig. 2. Case study 1 shows a head-to-head impact towards the front of the head around 15–50 degrees off centre to the right. This produced LOC with a high negative linear acceleration in the *x*-axis (forward and back) in the first 20 ms (Fig. 2A). High levels of strain were seen in many brain regions. These exceeded 1.5 times the group interquartile range (IQR) in all but two regions of interest. Case study 2 shows a head-to-head impact producing dystonic posturing. A high negative linear acceleration in the *y*-axis (right to left) was observed, with strains generally above the IQR but not exceeding 1.5 times the IQR in any regions of interest (Fig. 2B). Case study 3 shows a concussive head injury event involving a head-to-head impact to the left of the head that did not produce LOC or dystonic posturing. Negative linear acceleration was seen, predominantly in the *y*-axis, but the associated strains were below average in all brain regions (Fig. 2C).

Abnormal head kinematics producing loss of consciousness

We next tested for group differences in head kinematics (rotational/linear acceleration and velocity; Fig. 3A). A non-parametric Kruskal–Wallis H test was used with three levels (LOC, posturing and control impacts). These tests showed a significant main effect of group on peak linear acceleration [$H(2,79) = 11.3$, $P = 0.004$], peak rotational acceleration [$H(2,79) = 15.7$, $P < 0.001$] and peak rotational velocity [$H(2,79) = 7.4$, $P = 0.025$] (Fig. 3A). These differences were primarily the result of differences between LOC and control group

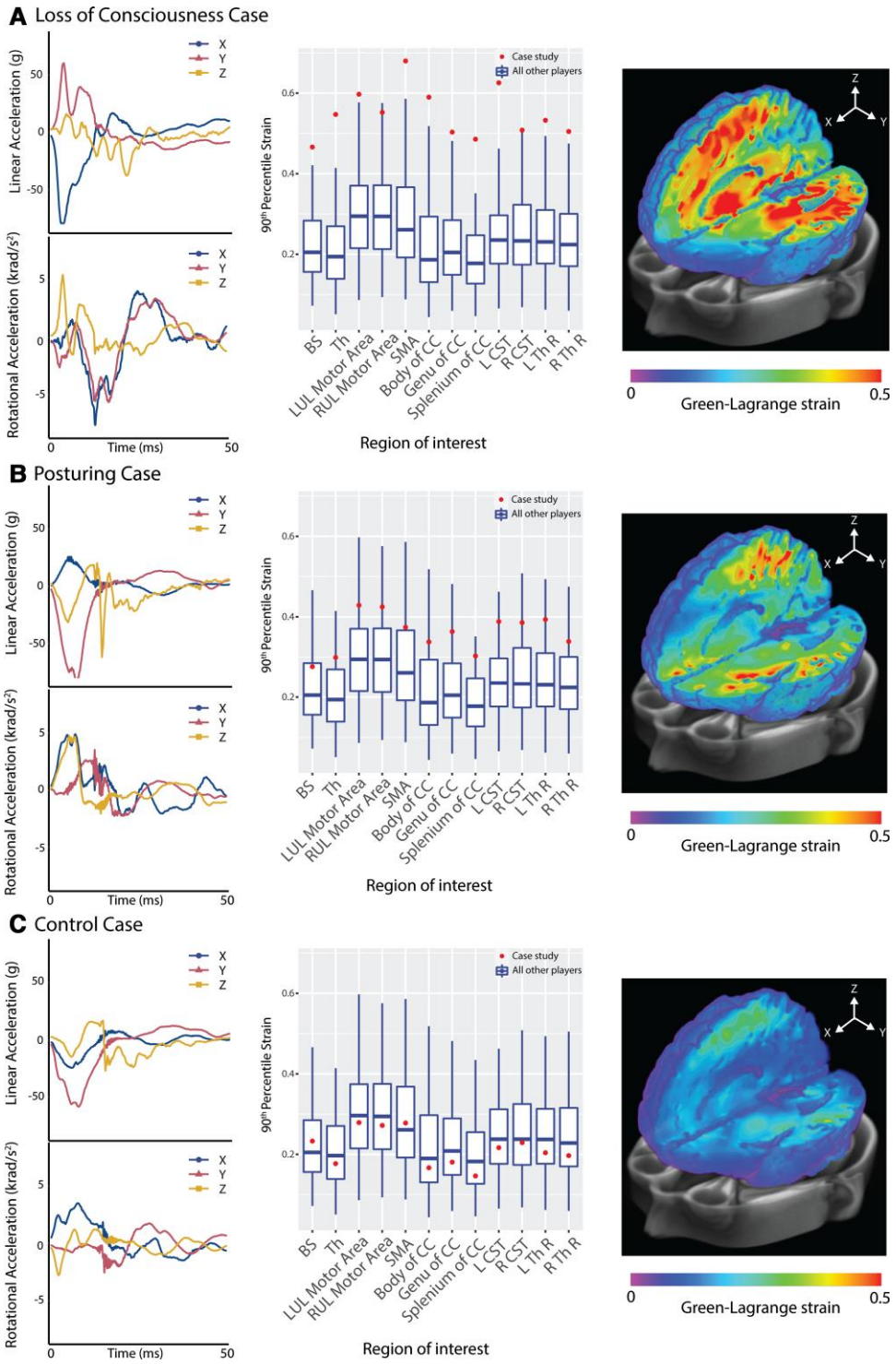

Figure 2 Case studies of injuries with different clinical features. Case studies of (**A**) LOC; (**B**) posturing; and (**C**) no neurological signs (control). The *left panel* shows head impact kinematics (linear and rotational acceleration). The *middle panel* shows the 90th percentile strain in brain regions of interest (individual = dot, box plots show median and IQR of all other impacts with whiskers indicating 1.5 times IQR). The *right panel* shows whole brain analysis of Green–Lagrange strain. BS = brainstem; CC = corpus callosum; CST = corticospinal tract; LUL = left upper limb; RUL = right upper limb; SMA = supplementary motor area; Th = thalamus; Th R = thalamic radiation.

impacts, with impacts leading to LOC associated with higher linear acceleration ($P = 0.004$) and rotational acceleration ($P < 0.001$), with borderline significance in rotational velocity ($P = 0.053$). Impacts leading to dystonic posturing also had higher rotational acceleration than control impacts ($P = 0.018$).

High brain strain and strain rates associated with loss of consciousness and posturing

Group changes in brain deformation were then assessed by estimating average strain and strain rates (Fig. 2B). As for head kinematics,

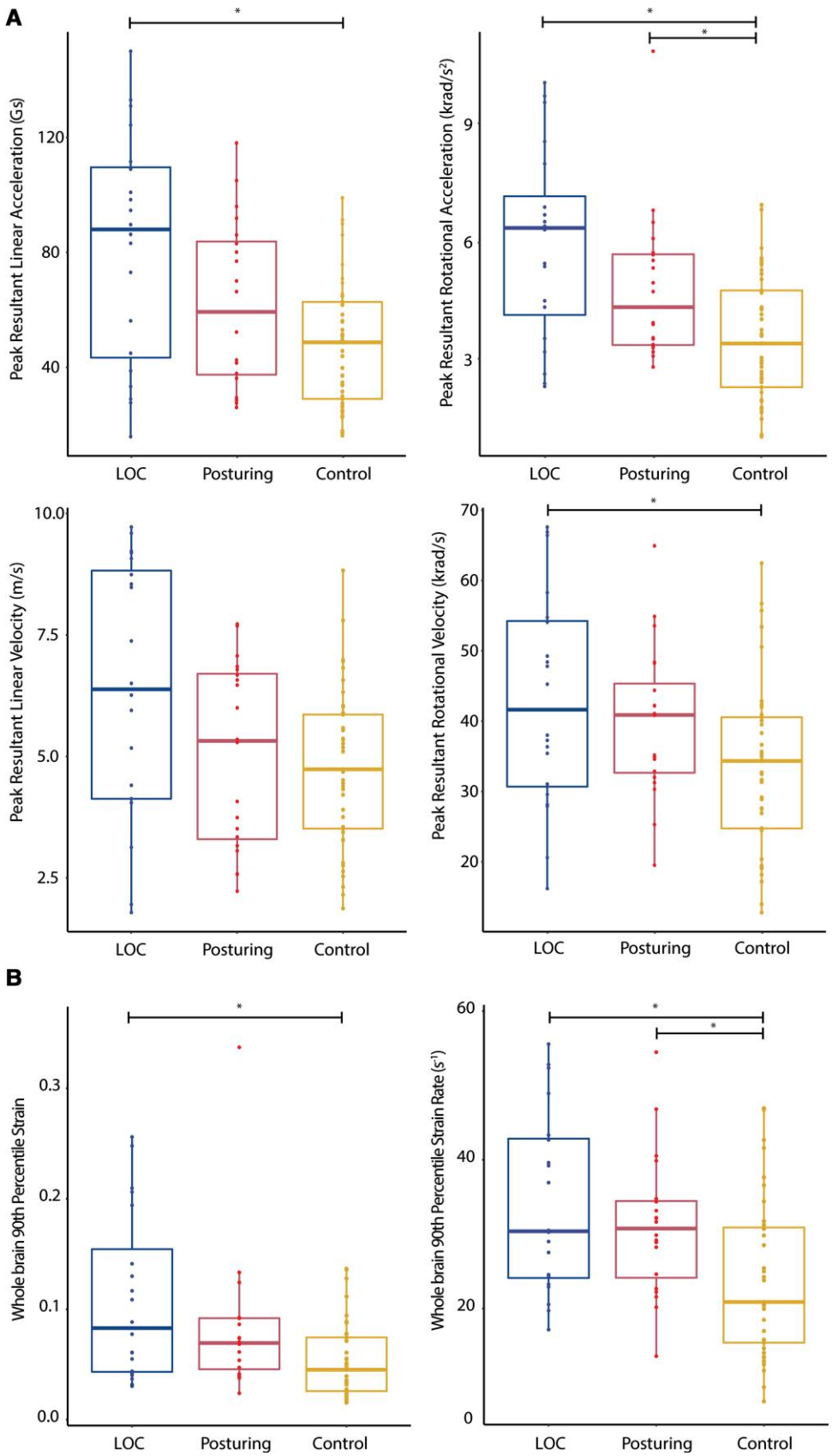

Figure 3 Kinematics and biomechanics of impacts. (**A**) Plots of rotational and linear acceleration and velocity; (**B**) Strain and strain rates for impacts leading to LOC (*left*), posturing (*middle*) or no visible signs (control, *right*). Format of box plots as in Fig. 2. Horizontal bars and asterisks highlight where groups are significantly different after *post hoc* testing ($P < 0.05$).

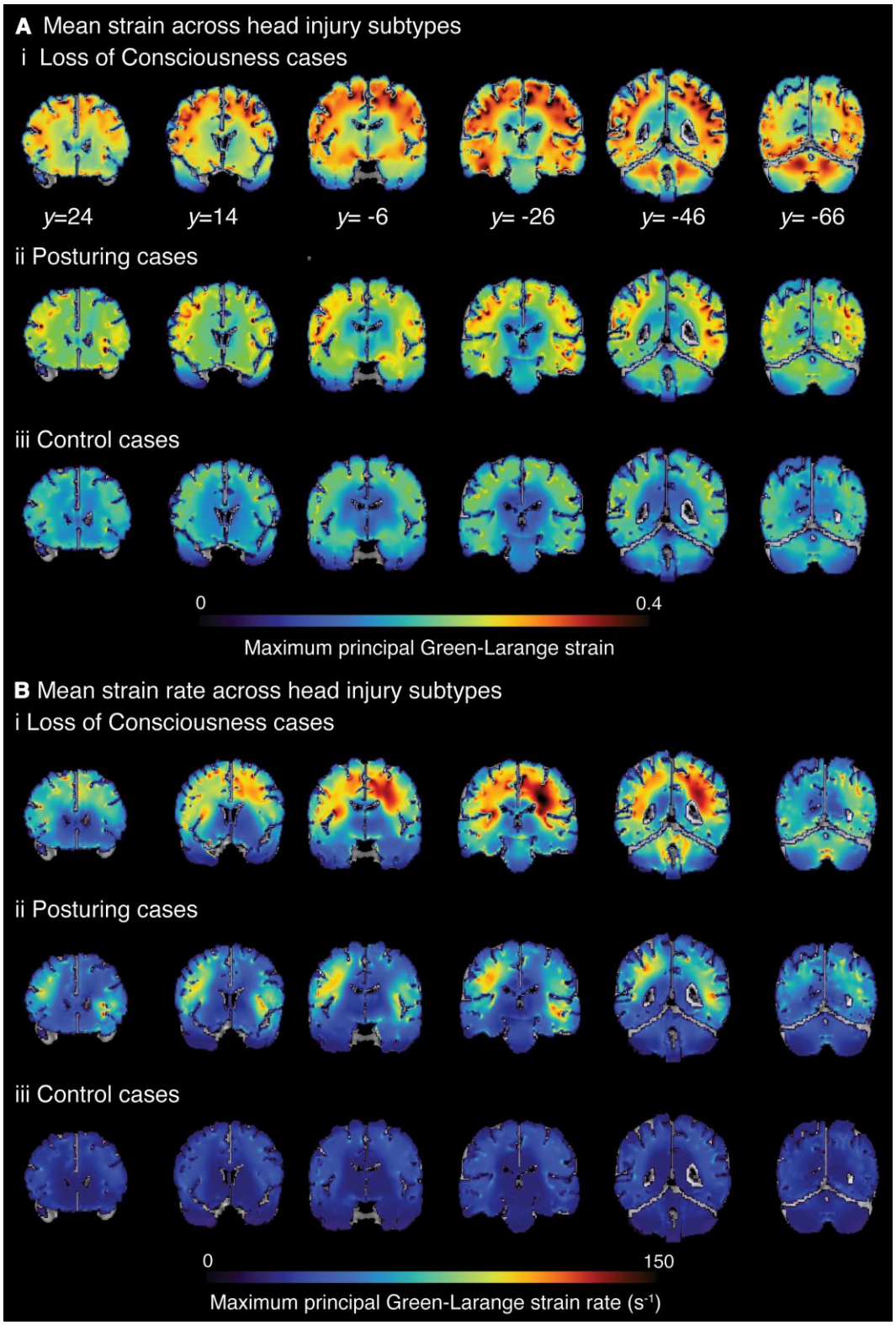

Figure 4 Spatial distribution of strain, strain rate across head injury subtypes. (**A**) The mean of maximum strain and (**B**) mean of maximum strain rate (s-1) across (i) LOC cases; (ii) posturing group; and (iii) control cases calculated for each voxel. *y* coordinates provided in MNI space.

there was a significant main effect of group in a non-parametric Kruskal–Wallis H test of 90th percentile strain [$H(2,79) = 11.8$, $P = 0.003$] and 90th percentile strain rate [$H(2,79) = 11.3$ $P = 0.004$]. Impacts leading to LOC had significantly higher strain ($P = 0.004$) and strain rate ($P = 0.010$) than control impacts. Both strain ($P = 0.031$) and strain rates ($P = 0.016$) were also higher in the posturing group compared to controls. Across the whole brain, 90th percentile strain and strain rates were highly correlated ($P < 0.001$, $r = 0.89$).

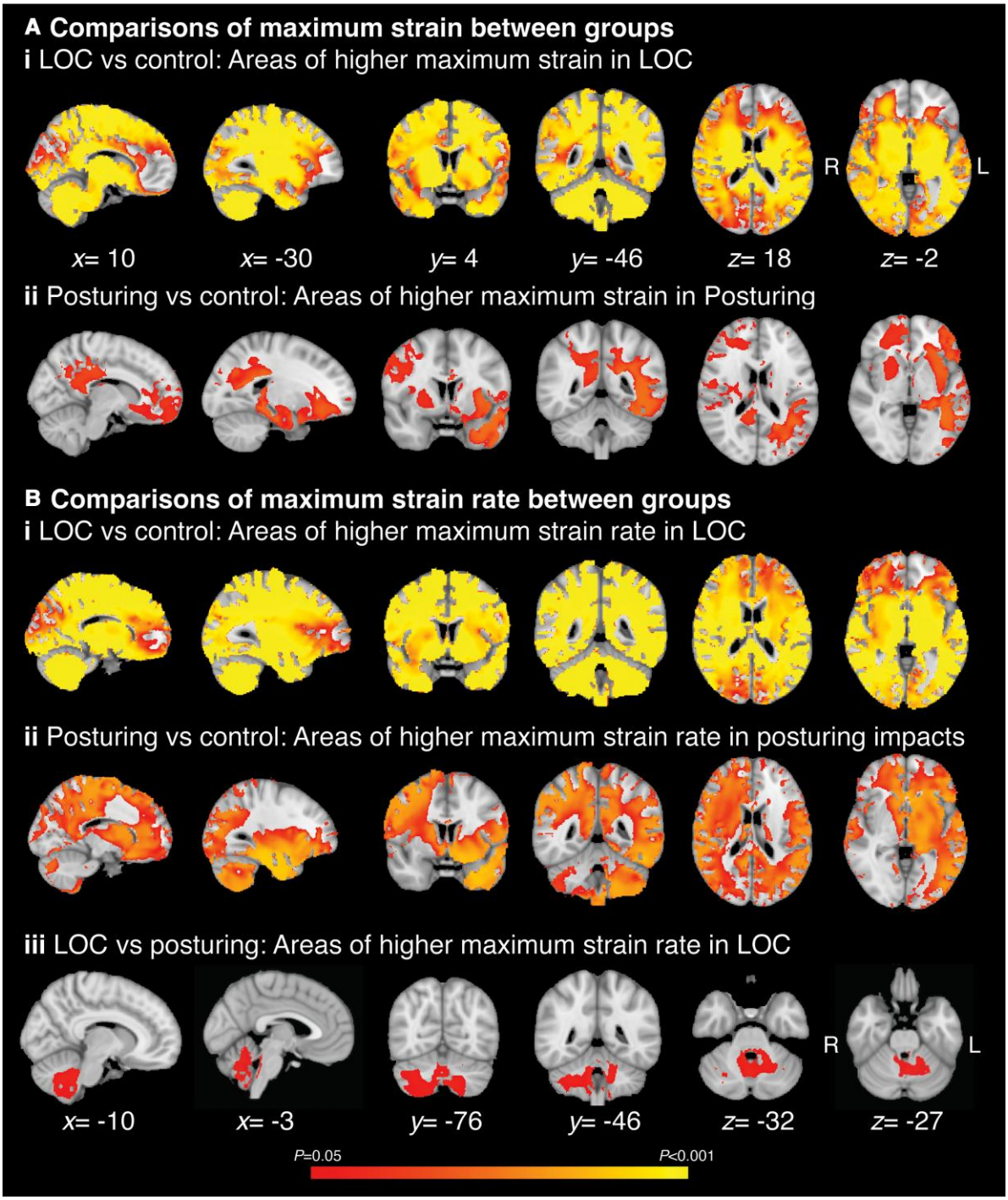

Figure 5 Areas of the brain with strain and strain rate differences across head injury subtypes. Voxel-wise analysis of strain and strain rates. (**A**) Areas of significantly higher maximum strain in (**i**) LOC compared to control group impacts; and (**ii**) posturing group compared to control group impacts. (**B**) Areas of significantly higher maximum strain in (**i**) LOC compared to control group impacts; (**ii**) posturing group compared to control group impacts; and (**iii**) LOC compared to posturing. Areas coloured are thresholded to indicate voxels which are significantly different between groups (TFCE corrected $P < 0.05$) across the brain. x, y and z coordinates provided in MNI space.

Voxel-wise maps of mean strain and strain rate showed distinct patterns of biomechanical effects as predicted by the FEM model. High mean strains and strain rates were apparent in many brain regions in LOC impacts [Fig. 4A(i) and B(i)]. Less pronounced strain and strain rates were seen in posturing group cases [Fig. 4A(ii) and B(ii)]. Strain was concentrated within the depths of the sulci bilaterally for all three event impact types, although concentration of forces in the sulci was less obvious for strain rate (Fig. 4B).

Directly comparing the groups showed distinct patterns of strain and strain rate for LOC and posturing groups. LOC compared to control impacts were associated with higher strain and strain rates in many brain regions, including the brainstem, cerebellum and many

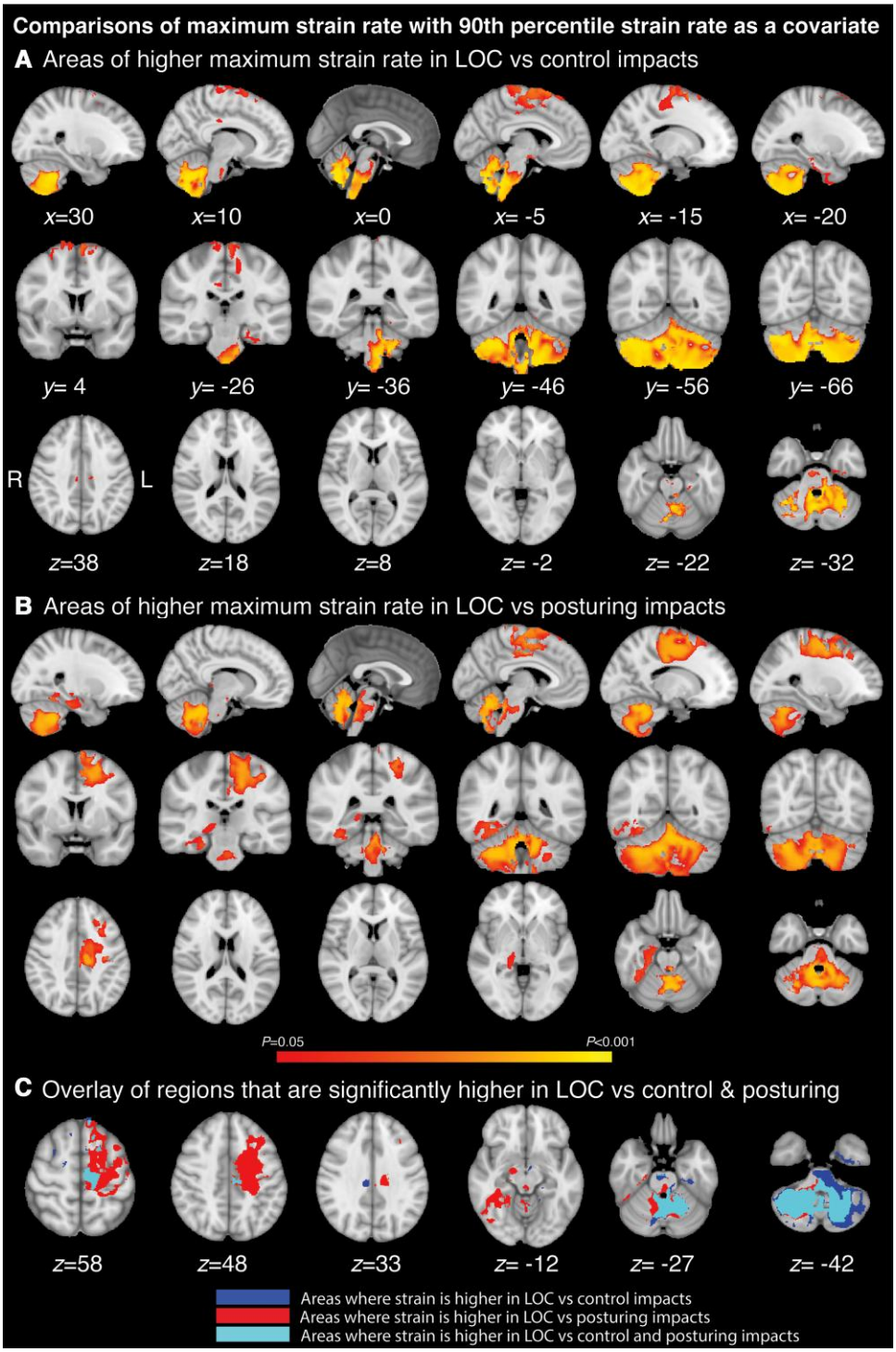

Figure 6 Strain rates associated with loss of consciousness controlling for overall biomechanical severity. Voxel-wise analysis including 90th percentile as a covariate. (**A**) Areas of increased strain rate for LOC compared control impacts; (**B**) Areas of increased strain rate for LOC compared to posturing impacts; (**C**) Overlay of increased strain rate for LOC versus posturing and control impacts. x, y and z coordinates provided in MNI space. Thresholding as in Fig. 5.

cortical regions except the frontal pole [Fig. 5 A(i) and B(i)]. Posturing impacts compared to controls showed less extensive strain increases, mainly seen in the left temporal lobe, left frontal orbital cortex, right putamen, right motor cortical regions and in white matter such as the body and splenium of the corpus callosum and left superior longitudinal fasciculus. Differences in strain were not observed in the cerebellum or brainstem [Fig. 5A(ii)]. Strain rates were also higher in the posturing group compared to control impacts, with increases in similar regions to those seen for strain but increases also seen in subcortical structures such as the thalamus, cerebellum and parts of the brainstem [Fig. 5B(ii)]. Region of interest analysis of strain and strain rates confirmed these observations (Supplementary Table 4).

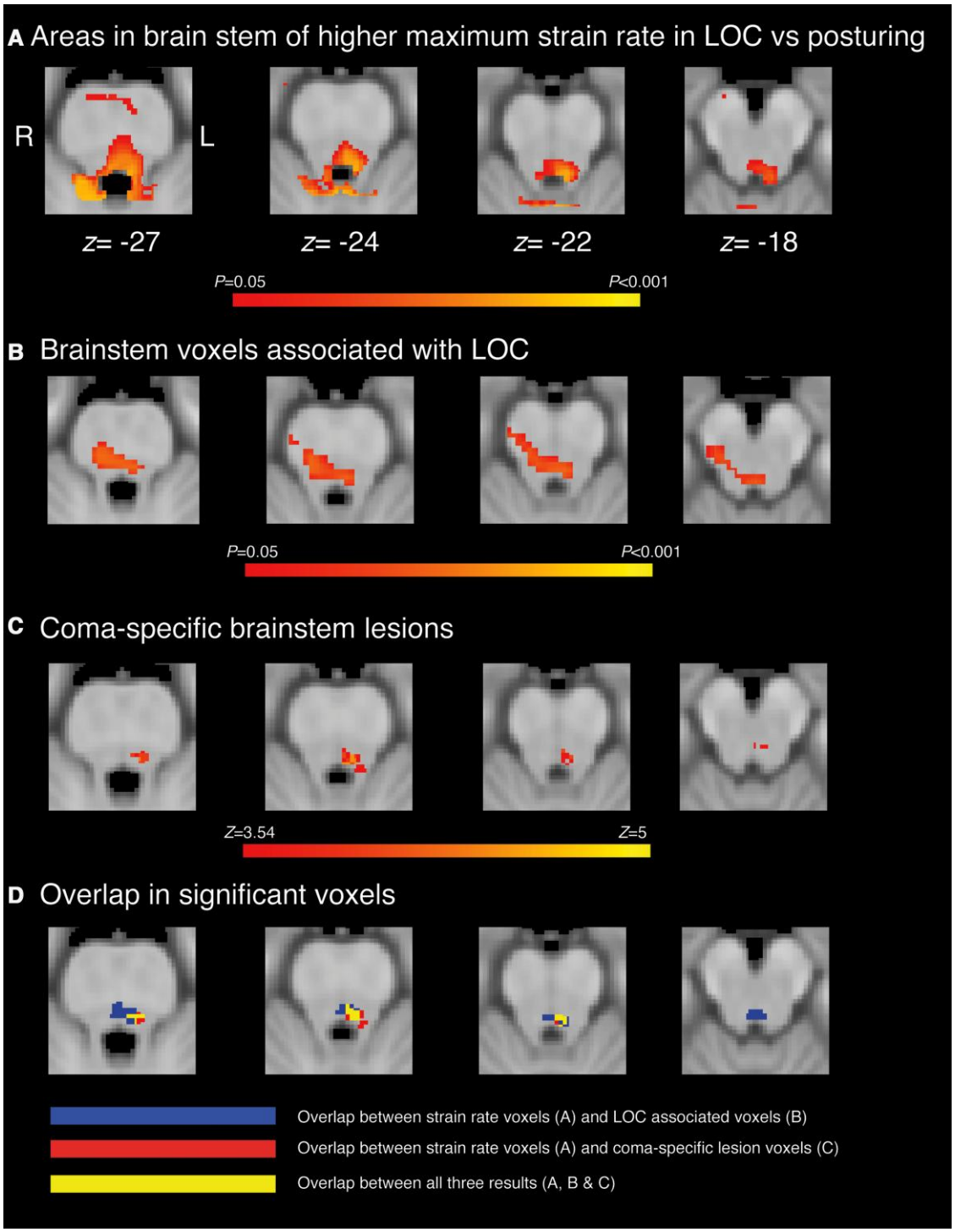

Figure 7 Overlap of strain rate differences with lesions associated with coma and LOC. (**A**) Areas of the brainstem with disproportionately higher strain rates in impacts with LOC compared with posturing impacts, compared with (**B**) lesions in the brainstem significantly associated with LOC ($P < 0.05$) from prior work[25] and (**C**) lesions significantly associated with brain-stem coma ($z > 3.54$) from prior work.[26] (**D**) Overlap between strain rate results (in **A**) with lesion maps from **B** (in blue) and **C** (in red). Yellow areas indicate overlap between all three maps. z coordinates are provided in MNI space.

Loss of consciousness is associated with high strain and strain rates in the brainstem and cerebellum

Loss of consciousness was associated with higher strain rates in the brainstem and cerebellum than posturing impacts [Fig. 5B(iii)]. The Harvard AAN atlas was used to evaluate brainstem nuclei affected.[60] This showed that the locus coeruleus, dorsal raphé, median raphé and parabrachial complex were likely to be affected. There were no differences in strain between the LOC and posturing groups.

We next controlled for the overall biomechanical severity of impact, as direct comparisons are potentially confounded by overall

differences in the magnitude of strain and strain rate between the groups. By using whole brain 90th percentile strain or strain rates as a covariate, this allows for spatial differences to be located regardless of the overall magnitude of strain. Proportionally higher strain rates were observed for LOC compared to controls in the cerebellum, pons and medulla of the brainstem and small areas of the motor cortex (Fig. 6A). These were observed in brainstem regions that included brainstem nuclei such as the pontis orealis, periaqueductal gray, locus coeruleus, dorsal raphé, median raphé and parabrachial complex, the left premotor cortex and the right temporal lobe (Fig. 6B). There were areas of overlap in the cerebellum, medulla and brainstem nuclei, including the locus coeruleus, dorsal raphé and parabrachial complex where strain rates were higher for the contrasts of LOC with posturing and control groups (Fig. 6C). There were no differences in proportional strain between any of the groups, or differences in strain rates observed between impacts leading to posturing and controls. There were also no regions where strain rate was disproportionally higher in control impacts or where posturing impacts showed higher strain or strain rate than LOC.

Finally, we investigated the spatial distribution of strain rates associated with LOC in comparison to previous reports of brainstem regions involved in LOC (Fig. 7). These studies used autopsy, CT or MRI to delineate different lesion types (vascular lesions of the brainstem versus cortical and subcortical lesions from penetrating head trauma) and together implicated the dorsal pontine tegmentum as being specifically associated with LOC (Fig. 7B and C).[25,26] Areas of increased strain rate associated with LOC in our study showed overlap with the dorsal pontine tegmentum, locus coeruleus and parabrachial complex (Fig. 7D).

Brain deformation and return to play duration

We assessed if brain deformation metrics were related to length of return to play duration. Impacts were grouped into leading to a return to play of less than 14 days, or 14 days or greater. Analysis of impact kinematics and brain deformation showed no differences between the groups (Supplementary Table 5).

Discussion

Our investigation of concussive head injuries show that specific patterns of biomechanical forces produced by head impacts are associated with distinct neurological impairments. We used a high-resolution computational model of head injury biomechanics to estimate the pattern of strain and strain rate produced by varying head impacts that had been reconstructed after video analysis. Advanced neuroimaging analysis techniques provided voxel-wise biomechanical estimates, allowing us to test specific hypotheses about the relationship between the anatomical location of strain and post-traumatic LOC and dystonic posturing. Whole brain strain and strain rates were high in a large number of brain regions following impacts leading to LOC. These included parts of the brainstem previously implicated in disorders of consciousness. After controlling for overall biomechanical severity, brain deformation was particularly seen in the cerebellum and brainstem. This overlapped with the location of brainstem lesions known to produce LOC, including the locus coeruleus, dorsal raphé and parabrachial complex. Less specific strain patterns were also seen in impacts producing dystonic posturing. This shows that quantifying the distribution of biomechanical forces in the brain produced by sporting head impacts informs the understanding of neurological signs and that head impacts may produce LOC through a biomechanical effect on key brainstem nuclei involved in the maintenance of consciousness.

Impacts producing LOC and those producing dystonic posturing were more biomechanically severe than control impacts. Higher levels of strain and strain rate were seen across widespread brain regions. The diffuse nature of the brain deformation may well be relevant to LOC, as distributed brain regions are involved in consciousness.[25] However, controlling for overall biomechanical severity allowed us to test whether strains and strain rates were more specifically related to LOC or dystonic posturing by comparing strain/strain rates across the groups, while accounting for individual differences in maximum strain/strain rates. This analysis showed no differences between posturing and control cases. In contrast, higher strain rates were present in LOC cases, specifically in brainstem and the cerebellum compared to impacts leading to either no visible signs or dystonic posturing. The dorsal brainstem was particularly affected. This region contains the locus coeruleus and dorsal raphé, which provide noradrenergic, dopaminergic and serotonergic projections to the cortex.[27,61] Strain rates were also high in areas overlapping the parabrachial complex, which projects to the thalamus, basal forebrain and other brainstem nuclei involved in consciousness.[27,62]

The location of high deformation in the dorsal raphé suggests that disruption of the arousal network is a potential mechanism for transient post-traumatic loss of consciousness. The locus coeruleus, dorsal raphé and parabrachial complex are involved in the control of arousal.[63-68] Recent work shows that photoinhibition of the parabrachial complex blocks hypocretin-mediated sleep-to-wake transitions, whilst stimulation of the locus coeruleus increased arousal.[69] Similarly, chemogenetic inhibition of dopaminergic neurones in the dorsal raphé reduces wakefulness, while optogenetic stimulation of these neurones promoted wakefulness.[65] Both the locus coeruleus and dorsal raphé neuron populations are disproportionately damaged following severe-TBI,[29] which is commonly associated with disorders of sleep and wakefulness.[70] Lesioning glutamatergic neurones in the parabrachial complex of rodents directly produced a comatose state.[63] Hence, high levels of biomechanical force in these nuclei during impacts may therefore interrupt ascending arousal signals, leading to LOC.

The way in which high strain impairs the ability of brainstem nuclei function remains unclear. Transient impairment of the arousal network might be produced either through direct compression or distortion of the brainstem itself or via shearing and distortion of axonal projections.[71,72] Axonal projections are particularly vulnerable to mechanical loading, including the shear, tensile and compressive forces that are generated as a result of mTBIs.[30-32] High biomechanical strains can produce this type of injury, because axons become brittle when force is applied rapidly,[73] particularly from rotational accelerations[40,74] of the head at the time of impact. LOC appears particularly related to rotational acceleration of the head, with impacts with purely linear acceleration components less likely to produce LOC.[75,76] Biomechanical forces are concentrated in upper parts of the brainstem due to it being relatively fixed within the posterior fossa in relation to the tentorium.[71] After TBI, white matter damage has particularly seen within the brainstem and thalamus of patients with long-term disorders of consciousness,[77-80] and the degree of this damage may correlate with the severity of impairment in consciousness.[81] Diffuse axonal injury affecting projections of the brainstem and thalamus may also disconnect the arousal system from cortical regions necessary for awareness, and play a critical role in producing prolonged disorders of consciousness.

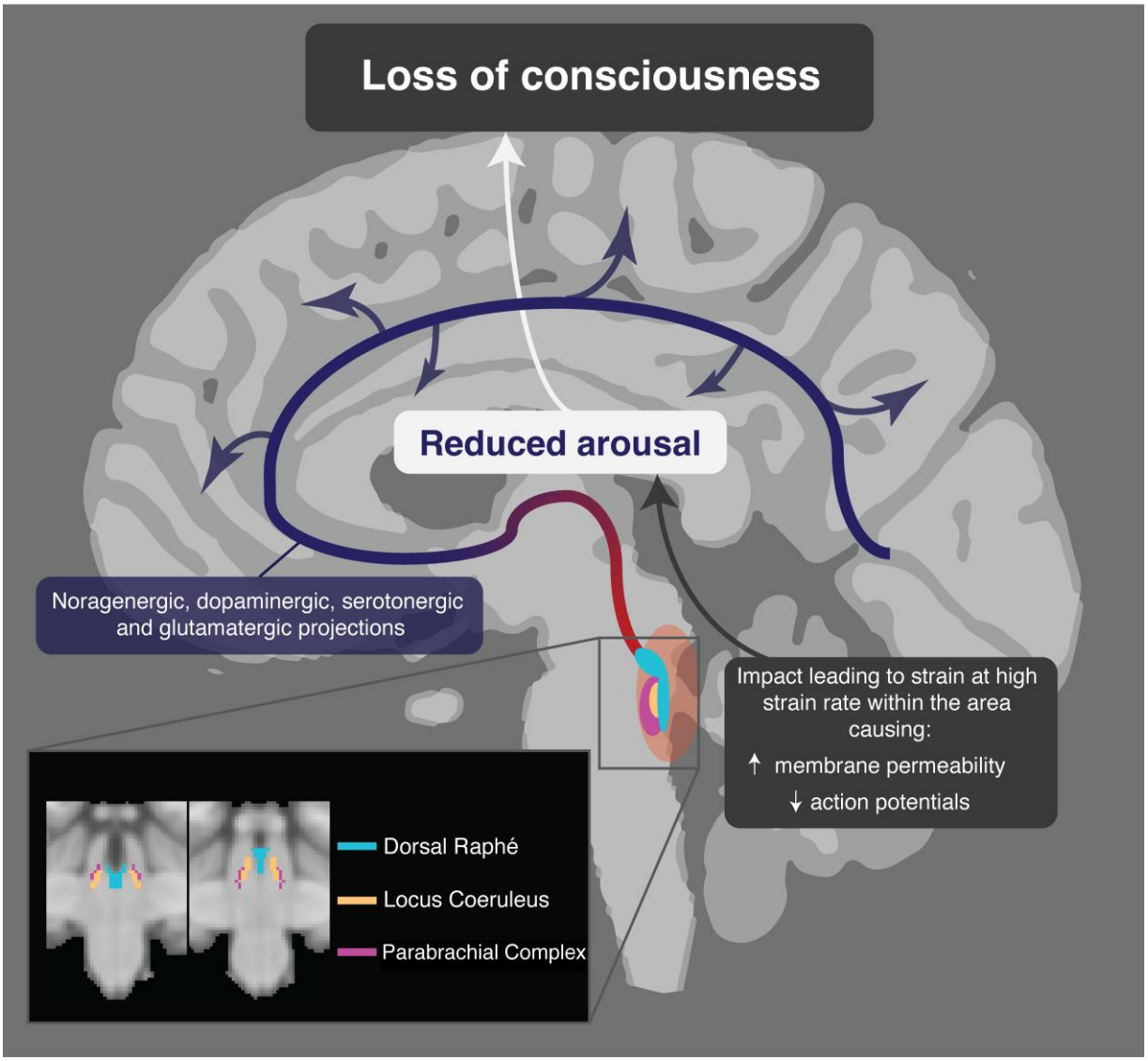

Figure 8 Proposed mechanism for traumatic loss of consciousness. High strain rates within the dorsal brainstem affect key arousal nuclei associated with arousal: the parabrachial complex, locus coeruleus and dorsal raphé. Axonal membrane disturbance temporarily impairs action potential firing, leading to transient reductions in noragenergic, dompaminergic, serotonergic and gulatamatergic projections (red-blue) to the cortex and subsequent LOC.

The transient nature of LOC suggests a physiological disruption in axonal function is likely, rather than a structural lesion. Animal neurophysiological studies are informative in this respect. Studies of rat and guinea pig spinal cord indicate that the degree of functional impairment, as measured by compound action potentials, is dependent on the strain rates, at strain similar to the levels observed in this study.[82,83] Disruptions of axonal membrane function and permeability are observed after high strain rates, which mainly resolve by 30 min, in keeping with the time course of LOC produced by head injury.[83,84] Hence, LOC produced by head injury observed could be the result of high strain rates to cause a disruption of axonal membrane function that exceeds the threshold necessary to temporarily disrupt of action potential propagation. Our results suggest that if high strain rates are locally concentrated within brainstem arousal nuclei, including the locus coeruleus, dorsal raphé and parabrachial complex, this may be sufficient to produce transient LOC (Fig. 8).

There are some limitations to our study. These partly relate to the use of video analysis and impact reconstruction methods. Video analysis carries a degree of error in estimation of velocity and angle of impacts that need to be considered, and the biofidelity of physical reconstruction and simulations depends on several factors including the anatomical fidelity of the head and neck, along with and fidelity of material models and properties. These limitations and how they are minimized are described in previous publications.[37-39,46] Nevertheless, these methods remain an important way to estimate the kinematics of the head and brain deformations during impacts in sport. The diagnosis of concussion in the cases we studied was made by medical professionals involved at the pitchside and could be influenced by some variation in diagnostic judgements. This is unlikely to have influenced our main findings as we focused on analysing the biomechanics of LOC and posturing, which were objectively quantified from video evidence. We analysed data from 2009–13 and did not require that an individual was only analysed in one of the experimental groups. Therefore, it is possible that multiple impacts from a single individual appeared in both control and non-control groups. This potential source of non-independence in the samples was not controlled for. Control impacts were selected to

be 'event matched' to the LOC and posturing groups, i.e. impacts with similar types of impact such as fall to the ground or shoulder-to-head collisions were included. We were able to control for differences in biomechanical confounders such as head impact location and injury severity. However, the players included in the three groups were not matched for demographic, prior head injury exposure or clinical information, because this was not available. It is possible that individual variability may have influenced the pattern of strain and strain rate we observed, and this is an important direction for future research. However, the players we studied were relatively homogenous, as they were all healthy professional athletes who were of similar age. Hence, the potential effects of extreme age or medical co-morbidities on the biomechanical effects of injury are unlikely to be relevant in this study group. We had limited access to clinical data from the post-traumatic effects of these injuries, which means we are unable to analyse the longer-term clinical effects of the impacts studied. Furthermore, the physical reconstruction methods and computational modelling did not consider physiological differences that may influence kinematics and brain deformations. Future studies should take into account the possibility of using the pipeline for generating the FE model on an individualized basis from subject MRI scans, which could be combined with advanced MRI such as diffusion tensor imaging of subjects to look at measures of white matter injury or structural connectivity.[42,85] We did not study any potential influence of repeated impacts within the game prior to the 'index' injury. It is possible that these are relevant to the occurrence of a concussive impact. Work using sensors systems such as instrumented mouthguards will enable research of this nature as they provide acceleration data throughout games and trainings without the need for video analysis or reconstruction[86] and can be paired with data science approaches that vastly reduce the time required to predict biomechanical forces within the brain.[87]

In conclusion, our study shows that impacts leading to LOC involve higher accelerations and velocities of the head, which in turn lead to higher levels of strain and strain rates within the brain. We show how novel brain injury biomechanics can be studied using advanced neuroimaging statistical tools. When coupled with a high-resolution computation model of brain injury biomechanics, this allows a detailed assessment of patterns of strain and strain rate produced by head impacts. In head impacts producing LOC, brain deformation is disproportionately seen in brainstem regions containing nuclei involved in arousal, including the locus coeruleus, dorsal raphé and parabrachial complex. This suggests that head impacts produce LOC through a biomechanical effect on key brainstem nuclei involved in the maintenance of consciousness.

Acknowledgements

M.G. acknowledges the support from Wellcome Trust (212430/Z/18/Z). K.A.Z. acknowledges support from ERA-NET Neuron. D.J.S. acknowledges support from his National Institute of Health Research (NIHR) Professorship Imperial College NIHR Biomedical Research Centre and the Care Research & Technology Centre, UK Dementia Research Institute.

Funding

The work was supported by a National Institute for Health and Care Research (NIHR) Research Professorship (D.J.S.) and the Care Research & Technology Centre, UK Dementia Research Institute.

Competing interests

D.J.S. is funded from the UK Dementia Research Institute and has received an honorarium from the Rugby Football Union for participation in an expert concussion panel, which was used to support his research. S.K. is employed as the Medical Services Director for the Rugby Football Union.

Supplementary material

Supplementary material is available at *Brain* online.

References

1. Maas AIR, Menon DK, Adelson PD, *et al*. Traumatic brain injury: Integrated approaches to improve prevention, clinical care, and research. *Lancet Neurol*. 2017;16:987-1048.
2. Davis GA, Makdissi M, Bloomfield P, *et al*. Concussion guidelines in national and international professional and elite sports. *Neurosurgery*. 2020;87:418-425.
3. Davis GA, Makdissi M, Bloomfield P, *et al*. International consensus definitions of video signs of concussion in professional sports. *Br J Sports Med*. 2019;53:1264-1267.
4. Smith DH, Meaney DF, Shull WH. Diffuse axonal injury in head trauma. *J Head Trauma Rehabil*. 2003;18:307-316.
5. Elkin BS, Morrison B. 3rd. Region-specific tolerance criteria for the living brain. *Stapp Car Crash J*. 2007;51:127-138.
6. Donat C, Yanez-Lopez M, Sastre M, *et al*. From biomechanics to pathology: Predicting axonal injury from patterns of strain after traumatic brain injury. *Brain*. 2021;144:70-91.
7. Guskiewicz KM, Mihalik JP. Biomechanics of sport concussion: Quest for the elusive injury threshold. *Exerc Sport Sci Rev*. 2011;39:4-11.
8. Cournoyer J, Hoshizaki TB. Head dynamic response and brain tissue deformation for boxing punches with and without loss of consciousness. *Clin Biomech (Bristol, Avon)*. 2019;67:96-101.
9. Cournoyer J, Hoshizaki TB. Biomechanical comparison of concussions with and without a loss of consciousness in elite American football: Implications for prevention. *Sports Biomech*. 2021;20:751-767.
10. Fuller GW, Kemp SP, Raftery M. The accuracy and reproducibility of video assessment in the pitch-side management of concussion in elite rugby. *J Sci Med Sport*. 2017;20:246-249.
11. Casson IR, Viano DC, Powell JW, Pellman EJ. Twelve years of national football league concussion data. *Sports Health*. 2010;2:471-483.
12. Echemendia RJ, Bruce JM, Meeuwisse W, Hutchison MG, Comper P, Aubry M. Can visible signs predict concussion diagnosis in the national hockey league? *Br J Sports Med*. 2018;52:1149-1154.
13. Gil C, Jacota M, Caudron Y, *et al*. How is video efficient to diagnose sport-related concussion? A cross-sectional study in the French TOP14 rugby championship. *Clin J Sport Med*. 2022;32(3):e261-e267.
14. Bruce SL, Dorney K. Posturing responses in concussions sustained by elite American football players. *Int J Athl Ther Train*. 2020;25:203-207.
15. Kuhl NO, Yengo-Kahn AM, Burnette H, Solomon GS, Zuckerman SL. Sport-related concussive convulsions: A systematic review. *Phys Sportsmed*. 2018;46:1-7.
16. McCrory PR, Berkovic SF. Video analysis of acute motor and convulsive manifestations in sport-related concussion. *Neurology*. 2000;54:1488-1491.
17. McCrory PR, Bladin PF, Berkovic SF. Retrospective study of concussive convulsions in elite Australian rules and rugby league

footballers: Phenomenology, aetiology, and outcome. *BMJ*. 1997; 314:171-174.
18. Iverson GL, Gardner AJ, Terry DP, *et al*. Predictors of clinical recovery from concussion: A systematic review. *Br J Sports Med*. 2017;51:941-948.
19. Collins MW, Iverson GL, Lovell MR, McKeag DB, Norwig J, Maroon J. On-field predictors of neuropsychological and symptom deficit following sports-related concussion. *Clin J Sport Med*. 2003;13:222-229.
20. Teel EF, Marshall SW, Shankar V, McCrea M, Guskiewicz KM. Predicting recovery patterns after sport-related concussion. *J Athl Train*. 2017;52:288-298.
21. Merritt VC, Greenberg LS, Meyer JE, Arnett PA. Loss of consciousness is associated with elevated cognitive intra-individual variability following sports-related concussion. *J Int Neuropsychol Soc*. 2021;27:197-203.
22. Wilde EA, Li X, Hunter JV, *et al*. Loss of consciousness is related to white matter injury in mild traumatic brain injury. *J Neurotrauma*. 2016;33:2000-2010.
23. Bremer F. *Cerveau "isolé" et physiologie du sommeil*. Masson; 1935.
24. Moruzzi G, Magoun HW. Brain stem reticular formation and activation of the EEG. *Electroencephalogr Clin Neurophysiol*. 1949;1: 455-473.
25. Snider SB, Hsu J, Darby RR, *et al*. Cortical lesions causing loss of consciousness are anticorrelated with the dorsal brainstem. *Hum Brain Mapp*. 2020;41:1520-1531.
26. Fischer DB, Boes AD, Demertzi A, *et al*. A human brain network derived from coma-causing brainstem lesions. *Neurology*. 2016; 87:2427-2434.
27. Parvizi J, Damasio AR. Neuroanatomical correlates of brainstem coma. *Brain*. 2003;126(Pt 7):1524-1536.
28. Zeman A. Consciousness. *Brain*. 2001;124(Pt 7):1263-1289.
29. Valko PO, Gavrilov YV, Yamamoto M, *et al*. Damage to arousal-promoting brainstem neurons with traumatic brain injury. *Sleep*. 1 2016;39:1249-1252.
30. Hill CS, Coleman MP, Menon DK. Traumatic axonal injury: Mechanisms and translational opportunities. *Trends Neurosci*. 2016;39:311-324.
31. Eierud C, Craddock RC, Fletcher S, *et al*. Neuroimaging after mild traumatic brain injury: Review and meta-analysis. *Neuroimage Clin*. 2014;4:283-294.
32. Jenkins PO, De Simoni S, Bourke NJ, *et al*. Dopaminergic abnormalities following traumatic brain injury. *Brain*. 2018;141: 797-810.
33. Hosseini AH, Lifshitz J. Brain injury forces of moderate magnitude elicit the fencing response. *Med Sci Sports Exerc*. 2009;41: 1687-1697.
34. McCrory PR, Berkovic SF. Concussive convulsions. Incidence in sport and treatment recommendations. *Sports Med*. 1998;25: 131-136.
35. Duckworth H, Azor A, Wischmann N, *et al*. A finite element model of cerebral vascular injury for predicting microbleeds location. *Front Bioeng Biotechnol*. 2022;10:860112.
36. Farajzadeh Khosroshahi S, Yin X, K Donat C, *et al*. Multiscale modelling of cerebrovascular injury reveals the role of vascular anatomy and parenchymal shear stresses. *Sci Rep*. 2021;11:12927.
37. Ghajari M, Hellyer PJ, Sharp DJ. Computational modelling of traumatic brain injury predicts the location of chronic traumatic encephalopathy pathology. *Brain*. 2017;140:333-343.
38. Zimmerman KA, Kim J, Karton C, *et al*. Player position in American football influences the magnitude of mechanical strains produced in the location of chronic traumatic encephalopathy pathology: A computational modelling study. *J Biomech*. 2021;118:110256.
39. Cournoyer J, Hoshizaki TB. Abnormal motor response associated with concussive injuries: Biomechanical comparison between impact seizures and loss of consciousness. *J Athl Train*. 2019;54:765-771.
40. Post A, Blaine Hoshizaki T, Gilchrist MD, Cusimano MD. Peak linear and rotational acceleration magnitude and duration effects on maximum principal strain in the corpus callosum for sport impacts. *J Biomech*. 2017;61:183-192.
41. Ho J, Kleiven S. Can sulci protect the brain from traumatic injury? *J Biomech*. 2009;42:2074-2080.
42. Anderson ED, Giudice JS, Wu T, Panzer MB, Meaney DF. Predicting concussion outcome by integrating finite element modeling and network analysis. *Front Bioeng Biotechnol*. 2020;8: 309.
43. Zhang L, Yang KH, King AI. Comparison of brain responses between frontal and lateral impacts by finite element modeling. *J Neurotrauma*. 2001;18:21-30.
44. Alshareef A, Giudice JS, Forman J, *et al*. Biomechanics of the human brain during dynamic rotation of the head. *J Neurotrauma*. 2020;37:1546-1555.
45. McCrory P, Meeuwisse W, Dvorak J, *et al*. Consensus statement on concussion in sport-the 5th international conference on concussion in sport held in Berlin, October 2016. *Br J Sports Med*. 2017;51:838-847.
46. Karton C, Blaine Hoshizaki T, Gilchrist MD. A novel repetitive head impact exposure measurement tool differentiates player position in national football league. *Sci Rep*. 2020;10:1200.
47. Post A, Koncan D, Kendall M, *et al*. Analysis of speed accuracy using video analysis software. *Sports Eng*. 2018;21:235-241.
48. Walsh ES, Kendall M, Post A, Meehan A, Hoshizaki TB. Comparative analysis of hybrid III neckform and an unbiased neckform. *Sports Eng*. 2018;21:479-485.
49. Chen Y, Ostoja-Starzewski M. MRI-based finite element modeling of head trauma: Spherically focusing shear waves. *Acta Mech*. 2010;213:155-167.
50. Dale AM, Fischl B, Sereno MI. Cortical surface-based analysis. I. Segmentation and surface reconstruction. *Neuroimage*. 1999;9:179-194.
51. Fischl B, van der Kouwe A, Destrieux C, *et al*. Automatically parcellating the human cerebral cortex. *Cereb Cortex*. 2004;14:11-22.
52. Alshareef A, Giudice JS, Forman J, Salzar RS, Panzer MB. A novel method for quantifying human in situ whole brain deformation under rotational loading using sonomicrometry. *J Neurotrauma*. 2018;35:780-789.
53. Holzapfel AG. *Nonlinear solid mechanics II*. Wiley;2000.
54. Winkler AM, Ridgway GR, Webster MA, Smith SM, Nichols TE. Permutation inference for the general linear model. *Neuroimage*. 2014;92:381-397.
55. Frazier JA, Chiu S, Breeze JL, *et al*. Structural brain magnetic resonance imaging of limbic and thalamic volumes in pediatric bipolar disorder. *Am J Psychiatry*. 2005;162:1256-1265.
56. Eickhoff SB, Paus T, Caspers S, *et al*. Assignment of functional activations to probabilistic cytoarchitectonic areas revisited. *Neuroimage*. 2007;36:511-521.
57. Oishi K, Zilles K, Amunts K, *et al*. Human brain white matter atlas: Identification and assignment of common anatomical structures in superficial white matter. *Neuroimage*. 2008;43: 447-457.
58. Hua K, Zhang J, Wakana S, *et al*. Tract probability maps in stereotaxic spaces: Analyses of white matter anatomy and tract-specific quantification. *Neuroimage*. 2008;39:336-347.
59. Fan L, Li H, Zhuo J, *et al*. The human brainnetome atlas: A new brain atlas based on connectional architecture. *Cereb Cortex*. 2016;26:3508-3526.

60. Edlow BL, Takahashi E, Wu O, *et al*. Neuroanatomic connectivity of the human ascending arousal system critical to consciousness and its disorders. *J Neuropathol Exp Neurol*. 2012;71:531-546.
61. Eban-Rothschild A, Appelbaum L, de Lecea L. Neuronal mechanisms for sleep/wake regulation and modulatory drive. *Neuropsychopharmacology*. 2018;43:937-952.
62. Benarroch EE. Parabrachial nuclear complex: Multiple functions and potential clinical implications. *Neurology*. 2016;86:676-683.
63. Fuller PM, Sherman D, Pedersen NP, Saper CB, Lu J. Reassessment of the structural basis of the ascending arousal system. *J Comp Neurol*. 2011;519:933-956.
64. Luo T, Yu S, Cai S, *et al*. Parabrachial neurons promote behavior and electroencephalographic arousal from general anesthesia. *Front Mol Neurosci*. 2018;11:420.
65. Cho JR, Treweek JB, Robinson JE, *et al*. Dorsal raphe dopamine neurons modulate arousal and promote wakefulness by salient stimuli. *Neuron*. 2017;94:1205-1219.e8.
66. Berridge CW. Noradrenergic modulation of arousal. *Brain Res Rev*. 2008;58:1-17.
67. Carter ME, Yizhar O, Chikahisa S, *et al*. Tuning arousal with optogenetic modulation of locus coeruleus neurons. *Nat Neurosci*. 2010;13:1526-1533.
68. Breton-Provencher V, Sur M. Active control of arousal by a locus coeruleus GABAergic circuit. *Nat Neurosci*. 2019;22:218-228.
69. Carter ME, Brill J, Bonnavion P, Huguenard JR, Huerta R, de Lecea L. Mechanism for hypocretin-mediated sleep-to-wake transitions. *Proc Natl Acad Sci U S A*. 2012;109:E2635-E2644.
70. Imbach LL, Valko PO, Li T, *et al*. Increased sleep need and daytime sleepiness 6 months after traumatic brain injury: A prospective controlled clinical trial. *Brain*. 2015;138(3):726-735.
71. Shaw NA. The neurophysiology of concussion. *Prog Neurobiol*. 2002;67:281-344.
72. Smith DH, Nonaka M, Miller R, *et al*. Immediate coma following inertial brain injury dependent on axonal damage in the brainstem. *J Neurosurg*. 2000;93:315-322.
73. Johnson VE, Stewart W, Smith DH. Axonal pathology in traumatic brain injury. *Exp Neurol*. 2013;246:35-43.
74. Meaney DF, Smith DH. Biomechanics of concussion. *Clin Sports Med*. 2011;30:19-31.
75. Gennarelli TA, Thibault LE, Ommaya AK. Pathophysiologic responses to rotational and translational accelerations of the head. *SAE Technical Paper*. 1972;1:720970.
76. Ommaya AK, Gennarelli TA. Cerebral concussion and traumatic unconsciousness. Correlation of experimental and clinical observations of blunt head injuries. *Brain*. 1974;97:633-654.
77. Gentry LR, Godersky JC, Thompson B. MR Imaging of head trauma: Review of the distribution and radiopathologic features of traumatic lesions. *AJR Am J Roentgenol*. 1988;150:663-672.
78. Moe HK, Moen KG, Skandsen T, *et al*. The influence of traumatic axonal injury in thalamus and brainstem on level of consciousness at scene or admission: A clinical magnetic resonance imaging study. *J Neurotrauma*. 2018;35:975-984.
79. Delano-Wood L, Bangen KJ, Sorg SF, *et al*. Brainstem white matter integrity is related to loss of consciousness and postconcussive symptomatology in veterans with chronic mild to moderate traumatic brain injury. *Brain Imaging Behav*. 2015;9:500-512.
80. Sandhu S, Soule E, Fiester P, *et al*. Brainstem diffuse axonal injury and consciousness. *J Clin Imaging Sci*. 2019;9:32.
81. Jang SH, Kwon YH. The relationship between consciousness and the ascending reticular activating system in patients with traumatic brain injury. *BMC Neurol*. 2020;20:375.
82. Singh A, Kallakuri S, Chen C, Cavanaugh JM. Structural and functional changes in nerve roots due to tension at various strains and strain rates: An in-vivo study. *J Neurotrauma*. 2009;26:627-640.
83. Shi R, Whitebone J. Conduction deficits and membrane disruption of spinal cord axons as a function of magnitude and rate of strain. *J Neurophysiol*. 2006;95:3384-3390.
84. Geddes DM, Cargill RS II, LaPlaca MC. Mechanical stretch to neurons results in a strain rate and magnitude-dependent increase in plasma membrane permeability. *J Neurotrauma*. 2003;20:1039-1049.
85. Jolly AB, Bălăeț M, Azor A, *et al*. Detecting axonal injury in individual patients after traumatic brain injury. *Brain*. 2020;144:92-113.
86. Liu Y, Domel AG, Yousefsani SA, *et al*. Validation and comparison of instrumented mouthguards for measuring head kinematics and assessing brain deformation in football impacts. *Ann Biomed Eng*. 2020;48:2580-2598.
87. Ghazi K, Wu S, Zhao W, Ji S. Instantaneous whole-brain strain estimation in dynamic head impact. *J Neurotrauma*. 2021;38:1023-1035.